

## Widenmannite, a rare uranyl lead carbonate: occurrence, formation and characterization

J. PLÁŠIL<sup>1,\*</sup>, J. ČEJKA<sup>1</sup>, J. SEJKORA<sup>1</sup>, P. ŠKÁCHA<sup>2</sup>, V. GOLIÁŠ<sup>2</sup>, P. JARKA<sup>2</sup>, F. LAUFEK<sup>3</sup>, J. JEHLÍČKA<sup>2</sup>, I. NĚMEC<sup>4</sup>  
AND L. STRNAD<sup>5</sup>

<sup>1</sup> Department of Mineralogy and Petrology, National Museum, Václavské náměstí 68, Praha 1, 115 79, Czech Republic

<sup>2</sup> Institute of Geochemistry, Mineralogy and Mineral Resources, Charles University in Prague, Faculty of Science, Albertov 6, Praha 2, 128 40, Czech Republic

<sup>3</sup> Czech Geological Survey, Geologická 6, Praha 5, 152 00, Czech Republic

<sup>4</sup> Department of Inorganic Chemistry, Charles University in Prague, Faculty of Science, Hlavova 2030, Praha 2, 128 40, Czech Republic

<sup>5</sup> Laboratories of the Geological Institutes, Charles University in Prague, Faculty of Science, Albertov 6, Praha 2, 128 40, Czech Republic

[Received 14 May 2008; Accepted 16-February 2010]

### ABSTRACT

The rare uranyl lead carbonate widenmannite,  $\text{Pb}_2(\text{UO}_2)(\text{CO}_3)_3$ , was found at the Janská vein, Příbram, Czech Republic, where two generations occur in several morphological types and mineral associations in hydrothermal veins. Alpha spectroscopy shows that these two generations have different ages, >220,000 and  $118 \pm 12$  y. ICP-MS analysis indicates that both widenmannites have a dominance of non-radiogenic Pb which originates from weathered galena. The older widenmannite I forms fine-grained, grey to beige aggregates in the highly altered supergene part of the hydrothermal ore vein in association with pyromorphite, cerussite and goethite. The younger widenmannite II occurs as white, yellow or greenish-yellow thin tabular crystals up to 0.5 mm long in association with cerussite, anglesite, limonite, kasolite and an unnamed Pb-U-O phase. Thermal analysis suggests that widenmannite decomposes in several steps, with Pb uranate as the final product. Infrared and Raman spectroscopy confirm the presence of non-equivalent  $(\text{CO}_3)^{2-}$  groups, bidentately coordinated in uranyl hexagonal polyhedra, forming the well known uranyl tricarbonato complex. Infrared spectroscopy shows conclusively that widenmannite does not contain molecular  $\text{H}_2\text{O}$ .

**KEYWORDS:** widenmannite, Příbram, thermal analysis, infrared spectroscopy, Raman spectroscopy, alpha spectroscopy, Pb isotopes.

### Introduction

WIDENMANNITE, a rare lead uranyl tricarbonato, with the ideal formula  $\text{Pb}_2(\text{UO}_2)(\text{CO}_3)_3$ , was described as a new mineral from the Michael mine in Weiler in Schwarzwald (Germany) by Walenta (1976). Two occurrences are 'Loe

Warren Zawn' (Elton and Hooper, 1995) and 'North Zawn', both at St. Just in Cornwall, UK (Elton and Hooper, 1996). A further widenmannite occurrence is described by Sejkora and Gabašová (1995) from Jáchymov, Czech Republic. Halls (2005) reports an occurrence of widenmannite from Hautajärvi, Lapin Laani, Finland, associated with uranophane, autunite and pyrite in uraniferous rocks. Carlson *et al.* (2007) described a widenmannite occurrence from the Huron River Uranium Prospect, Baraga County, Michigan, USA, in which widenmannite occurs in an assemblage of U and V minerals.

\* E-mail: jakub\_plasil@nm.cz

DOI: 10.1180/minmag.2010.074.1.97

The widemannite in this study was found during research into the alteration processes of base-metal and U mineralization of the Jánská vein (Škácha *et al.*, 2009; Plášil *et al.*, 2010). The Jánská vein is one of the minor veins of the famous base-metal deposit Březové Hory, Příbram, Central Bohemia, Czech Republic. Investigations have shown that two generations of widemannite are present on the vein, a suggestion that was later supported by radiometric methods determining their ages. The present study was undertaken with a view to quantifying rigorously the ages of the two widemannite phases, to report the compositional variation of widemannite, and to present a thorough characterization using vibrational spectroscopy from which conclusions relating to the uranyl group and H<sub>2</sub>O could be derived. The rarity of the mineral and the very limited mineralogical data available prompted us to examine it in detail.

### Characteristics of widemannite occurrence

Widemannite is found in the 'Jánská vein', which is a minor hydrothermal vein of the base-metal deposit at Březové Hory near Příbram, Czech Republic. The ore deposit lies within the Cambrian rocks of the Teplá–Barrandian zone of the Bohemian Massif. The vein was exploited for the locally developed Ag mineralization. The Jánská vein is also noted for its U mineralization, which is an unusual feature in the Březové Hory ore district, and has been documented since the 19<sup>th</sup> century. Uranium mineralization is represented by massive uraninite and so-called 'gummite' – mostly amorphous Pb-U oxides and hydroxides (Reuss, 1859, 1863; Babánek, 1872) along with cuprosklodowskite, metatorbernite, masuyite, wölsendorfit, anglesite and zippeite (Ondruš and Hyršl, 1989).

Recent research has revealed rich aggregates of kasolite (Škácha and Sejkora, 2001), zinc-zippeite (Sejkora *et al.*, 2003), compreignacite, uranopilite and uranophane (Plášil *et al.*, 2005). Škácha and Plášil (2002) describe the mineralogy of the Březové Hory deposit and mention briefly the widemannite occurrence, while Plášil *et al.* (2003) reviewed the detailed mineralogy of the Jánská vein itself.

Two types of widemannite occur in the vein. Generally, they can be divided as follows:

(1) An older generation of widemannite, so-called widemannite I, which forms grey to beige, massive aggregates with conchoidal fracture. It

occurs at the first level of the Prokop shaft in association with pyromorphite, cerussite and goethite;

(2) A younger generation, so-called widemannite II, occurs at the second level of the Prokop shaft in several complex associations and habits including: (i) yellow to greenish-yellow spherical aggregates comprising fine thick tabular crystals in sphalerite veinlets with galena and uraninite; these aggregates, which cover several cm<sup>2</sup>, are often overgrown by grey tabular crystals of cerussite; (ii) commonly, as light yellow, long tabular crystals up to 0.5 mm, forming isolated spherical aggregates which were found on a fracture of galena vein covered by limonite in close association with greenish-yellow crystalline aggregates of anglesite and thick tabular aggregates of cerussite, locally covered by limonite; (iii) rarely, as thin tabular crystals, strongly elongated along the *c* axis, covering fractures in galena veins with uraninite together with U oxides and kasolite (Fig. 1); (iv) hedgehog-like aggregates of light green to yellow colour on fractures in highly altered uraninite together with 'gummite', kasolite and orange tabular aggregates of the Pb-U-O phase, a study of which is not presented here.

The old adit, where widemannite II was found, is dated by its face advance at the end of 19<sup>th</sup> century (~1890).

### Experimental methods

#### X-ray diffraction

The X-ray diffraction experiments on a single-crystal diffractometer were not successful. Powder X-ray diffraction data were collected using a PANalytical X'Pert Pro powder diffractometer with a silicon solid-state X'Celerator detector operating at 40 kV and 30 mA. A

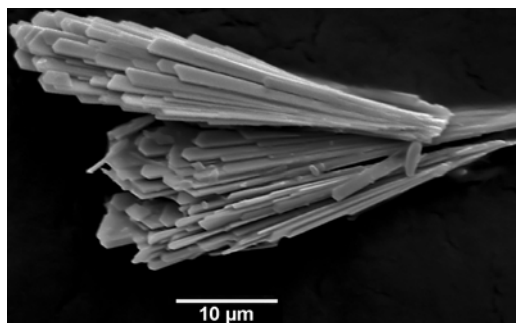


FIG. 1. SEM image. Fine twinned parallel crystals of widemannite II. (Jeol JSM-6380).

secondary graphite (002) monochromator was used to produce Cu- $K\alpha_{1,2}$  radiation. The diffraction patterns were collected in the range  $10\text{--}90^\circ 2\theta$  with a step-size of  $0.02^\circ 2\theta$  and counting time of 5.5 s per step. The powder samples were placed onto zero-background silicon wafers from a suspension of acetone. The diffraction patterns obtained were analysed using *High-Score* (PANalytical). The position and intensity of each peak were refined using a Pearson VII line-shape function by the *Xfit* program (Cheary and Coelho, 1996). The program *HKLgen* (Le Bail, 1998) was used for calculating a theoretical diffraction pattern (peak positions only). The unit-cell parameters were refined by the program of Burnham (1962) based on a least-squares method.

#### Chemical study and thermal analysis

Quantitative chemical data were obtained using the Cameca SX100 electron microprobe at the Joint Laboratory of Masaryk University and Czech Geological Survey, Brno. Samples were set in an epoxy resin disc and polished. Wavelength-dispersive spectrometry was used with an operating voltage of 15 kV, 4 nA probe current and  $10\ \mu\text{m}$  final beam diameter. The following X-ray lines, analysing crystals and standards were selected for analysis:

$K\alpha$  lines were used for the determination of F (PC1, fluorapatite), V (LLIF, vanadinite), P (LPET, fluorapatite), Fe (LLIF, andradite), Zn (LLIF, ZnO), Al (TAP, sanidine), Si (TAP, sanidine), S (PET, baryte) and Ca (PET, andradite);

$L\alpha$  lines were used in the determination of Cu (TAP, diopside) and As (TAP, InAs), and the  $L\beta$  line for Ba (LPET, baryte);

$M\alpha$  lines were used in the determination of: Pb (PET, vanadinite), and  $M\beta$  lines were used for Bi (LPET, Bi metal) and U (LPET,  $\text{UO}_2$ ).

Peak counting times used for major and minor elements were 20 and 60 s respectively. Background counting times were half the peak time. Counts were transformed into concentrations using the 'PAP' program (Pouchou and Pichoir, 1985). The contents of Al, As, Ba, Bi, Ca, Cu, F, Fe, P, S, Si and V were found to be below the detection limit ( $\sim 0.01\text{--}0.05$  wt.%).

Thermal analysis of the widenmannite II sample was performed on a Stanton Redcroft Thermobalance TG 750, heating rate  $10^\circ\text{C min}^{-1}$ , dynamic air atmosphere, flow rate  $10\ \text{ml min}^{-1}$ , sample weight 0.82 mg.

#### Vibrational spectroscopy

The infrared (IR) spectrum of the widenmannite II (in mixture with powder KBr without using pressure) was recorded by a micro-diffuse reflectance method (DRIFTS) on a Nicolet Magna 760 FTIR spectrometer (range  $4000\text{--}600\ \text{cm}^{-1}$ , resolution  $4\ \text{cm}^{-1}$ , 256 scans, Happ-Genzel apodization) equipped with a Spectra Tech InspectIR micro-FTIR accessory. Raman spectroscopy of fine crystals was performed on a multichannel Renishaw *InVia*/Reflex microspectrometer coupled with a Peltier-cooled CCD detector. Excitation was provided by the 514.5 nm line of a continuous-wave 10 mW Ar-ion laser (the laser was used at 50% of its power). The samples were scanned from 100 to  $4000\ \text{cm}^{-1}$  at a spectral resolution of  $2\ \text{cm}^{-1}$ . The counting time for each Raman spectrum acquisition was 10 s and 10 scans were accumulated for each experimental run to provide a better signal-to-noise ratio. Multiple spot analyses on different areas of the same sample provided similar spectra and confirmed the reproducibility of spectra.

#### Lead isotopes

Lead isotopic data were obtained by means of ICP-MS. Each sample was digested in 10 ml 65%  $\text{HNO}_3$  in PTFE vessels (Savillex, USA) overnight on a hot plate ( $150^\circ\text{C}$ ). After the vessel was opened, the sample was evaporated to  $\sim 0.5$  ml of the digest, which was then dissolved in 2%  $\text{HNO}_3$  and transferred to a volumetric flask. All the samples and experimental blanks were further diluted by 2% (v/v)  $\text{HNO}_3$ . All the chemicals used in the dissolution were reagent grade (Merck, Germany) and the acids were double-distilled. Deionized water from a Millipore system was used for all dilutions. All solutions were stored in HDPE (Nalgene) bottles. A similar procedure was used for the decomposition of geological samples by Strnad *et al.* (2005). The  $^{207}\text{Pb}/^{206}\text{Pb}$  and  $^{208}\text{Pb}/^{206}\text{Pb}$  isotopic composition was determined using a standard configuration of quadrupole-based ICP-MS PQ3 (VG Elemental, UK) equipped with a water-cooled ( $\sim 4^\circ\text{C}$ ) spray chamber with Meinhard-type nebulizer. The analytical conditions and data acquisition parameters followed closely those described by Mihaljevič *et al.* (2006). The data were acquired in the peak-jumping mode with 4 points measured per mass peak and with an instrument sensitivity of  $3 \times 10^4$  cps per  $1\ \text{ng ml}^{-1}$   $^{209}\text{Bi}$ . The total

acquisition time was  $10 \times 30$  s. Correction for the mass bias was performed using NIST SRM 981 (a common Pb isotopic standard) and SRM 982 (an equal atom Pb isotopic standard) after every analysed sample and the time-resolved data were processed offline using Microsoft Excel™. The standard errors for measurements of the  $^{207}\text{Pb}/^{206}\text{Pb}$  and  $^{208}\text{Pb}/^{206}\text{Pb}$  were below 0.5% (relative). The accuracy of the measurements was controlled by repeated analysis of the AGV-2 (USGS, USA;  $^{207}\text{Pb}/^{206}\text{Pb} = 1.2085 \pm 0.0006$ ,  $^{208}\text{Pb}/^{206}\text{Pb} = 2.0415 \pm 0.0013$ ).

### Alpha Spectroscopy

Alpha spectrometry was used for radioactive equilibrium determination and subsequent dating of widemannite samples. Data were collected on a CANBERRA PIPS 450 mm<sup>2</sup> semiconductor detector with an ORTEC 142A pre-amplifier and a CANBERRA DSA2000 multichannel analyzer controlled by GENIE2000 software. The sample powder was deposited from the water suspension onto a polished 22 mm stainless steel disc, evaporated and weighed. This non-destructive method (Jarka, 2007) is a modified procedure of the one described by Killeen and Carmichael (1976). Reference materials CRM 129-A (natural U oxide, isotopic) and BL-5 (U ore) were used. To

separate U and Th the fractions-modified method of Maxwell (1998), as described by Jarka (2007) and also reported in *Eichrom* technical papers (www.eichrom.com), was used. The sample in the solution with HNO<sub>3</sub> of aliquot activity 1 Bq was spiked by the  $^{232}\text{U}/^{228}\text{Th}$  of equal activity. The sample was evaporated close to dryness, dissolved in 0.5M Al(NO<sub>3</sub>)<sub>3</sub> and 4 M HNO<sub>3</sub> and sorbed onto activated UTEVA<sup>®</sup> chromatographic exchange resin. The Th fraction was stripped by 5 ml of 6 M HCl and then U by 15 ml of 0.02 M HCl. Individual fractions were evaporated and diluted in 0.3 M Na<sub>2</sub>SO<sub>4</sub> and H<sub>2</sub>SO<sub>4</sub> buffer at pH 1.6. Thorium and U targets were produced over 1 h by electrodeposition onto a polished stainless steel disc (using a current density of 0.22 A cm<sup>-2</sup>) and subsequently measured by alpha spectrometry. The measurements of HU-1 (Harwell uraninite) standard verified the obtained results giving following equilibrium:  $^{234}\text{U}/^{238}\text{U} 1.020 \pm 0.065$  and  $^{230}\text{Th}/^{234}\text{U} 0.984 \pm 0.068$  ( $2\sigma$ ).

## Results

### X-ray diffraction

The X-ray powder diffraction pattern of widemannite II is reported in Table 1. The refined unit-cell parameters,  $a = 8.960(2)$  Å,  $b = 9.381(2)$  Å,  $c = 5.001(3)$  Å and  $V = 420.4(2)$  Å<sup>3</sup>

TABLE 1. Powder diffraction data for widemannite II from Příbram.

$I_{\text{(rel.)}}$	$d_{\text{(obs.)}}$	$d_{\text{(calc.)}}$	$h$	$k$	$l$	$I_{\text{(rel.)}}$	$d_{\text{(obs.)}}$	$d_{\text{(calc.)}}$	$h$	$k$	$l$
3	6.481	6.479	1	1	0	<b>15</b>	<b>1.8820</b>	<b>1.8785</b>	<b>3</b>	<b>1</b>	<b>2</b>
6	4.693	4.691	0	2	0	4	1.8445	1.8446	3	4	0
4	4.425	4.413	0	1	1	4	1.8208	1.8210	4	3	0
<b>68</b>	<b>4.157</b>	<b>4.156</b>	<b>1</b>	<b>2</b>	<b>0</b>	1	1.7915	1.7920	5	0	0
<b>8</b>	<b>4.044</b>	<b>4.043</b>	<b>2</b>	<b>1</b>	<b>0</b>	1	1.7753	1.7748	3	2	2
1	3.959	3.959	1	1	1	6	1.7306	1.7306	3	4	1
<1	3.346	3.337	2	0	1	6	1.7306	1.7306	2	5	0
<b>18</b>	<b>3.240</b>	<b>3.240</b>	<b>2</b>	<b>2</b>	<b>0</b>	4	1.6855	1.6870	5	0	1
7	3.142	3.144	2	1	1	3	1.6427	1.6427	4	1	2
6	2.987	2.987	3	0	0	4	1.5885	1.5874	5	2	1
7	2.953	2.952	1	3	0	4	1.5885	1.5887	3	5	0
2	2.846	2.846	3	1	0	1	1.5531	1.5548	5	3	0
5	2.559	2.564	2	3	0	5	1.5406	1.5410	4	4	1
7	2.519	2.519	3	2	0	3	1.4856	1.4847	5	3	1
<b>100</b>	<b>2.346</b>	<b>2.345</b>	<b>0</b>	<b>4</b>	<b>0</b>	4	1.4762	1.4748	6	1	0
2	2.240	2.240	4	0	0	<b>9</b>	<b>1.4230</b>	<b>1.4230</b>	<b>2</b>	<b>5</b>	<b>2</b>
2	2.179	2.183	2	0	2	2	1.3853	1.3852	3	6	0
2	2.160	2.160	3	3	0	<1	1.2398	1.2400	7	0	1
2	2.125	2.127	2	1	2	3	1.1728	1.1726	0	8	0

## WIDENMANNITE FROM PŘÍBRAM, CZECH REPUBLIC

TABLE 2. Unit-cell parameters of widenmannite.

	Widenmannite I (this paper)	Widenmannite II (this paper)	Elton and Hooper (1995)	Walenta (1976)
$a$ (Å)	8.964(4)	8.960(2)	8.971(3)	8.99
$b$ (Å)	9.378(6)	9.381(2)	9.381(3)	9.36
$c$ (Å)	5.007(4)	5.001(3)	5.002(2)	4.95
$V$ (Å <sup>3</sup> )	420.9(4)	420.4(2)	421	417

are slightly larger than those reported by Walenta (1976) but comparable to those given by Elton and Hooper (1995), (Table 2). Systematic absences noted among the available reflections ( $0kl: k+l=2n+1; 00l: l=2n+1; 0k0: k=2n+1$ ) are consistent with the space groups  $Pnmm$  (No. 59),  $Pnm2_1$  (No. 31) and  $P22_12_1$  (No. 18). X-ray powder diffraction patterns of widenmannites I and II are very similar. Widenmannite I exhibits differences in intensities in comparison with widenmannite II but the unit-cell parameters are similar:  $a = 8.964(4)$  Å,  $b = 9.378(6)$  Å,  $c = 5.007(4)$  Å,  $V = 420.9(4)$  Å<sup>3</sup>.

*Chemical study and thermal analysis*

The empirical formula of widenmannite I calculated from the average results of 4 spot analyses and based on  $Pb+Fe+Zn+U = 3$  a.p.f.u. is  $(Pb_{1.92}Fe_{0.09}Zn_{0.01})_{\Sigma 2.02}(UO_2)_{0.98}(CO_3)_{2.95}$  (Table 3). Here, along with the major contents of Pb, notable concentrations of Fe were detected. The valence state of Fe is open to question but it can be assumed it should be Fe<sup>2+</sup> to preserve the homovalent substitution. No Fe<sup>3+</sup>-bearing uranyl carbonate is known, either in nature or as the synthetic compound. The average empirical formula of widenmannite II calculated from the

TABLE 3. Chemical composition of widenmannite I.

	1	2	3	4	Mean	Ideal
FeO	0.72	0.87	0.52	0.96	0.77	0.00
PbO	47.98	48.93	50.66	48.66	49.06	51.64
ZnO	0.11	0.11	0.08	0.04	0.09	0.00
UO <sub>3</sub>	31.82	32.52	31.97	32.64	32.24	33.09
CO <sub>2</sub> *	14.68	15.00	14.75	15.08	14.88	15.27
Total	95.31	97.43	97.99	97.39	97.03	100.00
Formulae based on $\Sigma(Pb+Fe+Zn+U) = 3$						
Fe	0.089	0.105	0.063	0.116	0.093	0.000
Pb	1.911	1.899	1.962	1.890	1.916	2.000
Zn	0.012	0.012	0.008	0.005	0.009	0.000
$\Sigma A$ site	2.012	2.016	2.033	2.011	2.018	2.000
U	0.989	0.985	0.966	0.989	0.982	1.000
C*	2.965	2.952	2.897	2.971	2.946	3.000
$\Sigma(U+C)$	3.953	3.936	3.864	3.960	3.928	4.000
Pb/U	1.93	1.93	2.03	1.91	1.95	2.00

Mean: calculated from the 4 representative point analyses (1–4).

Ideal: theoretical composition of widenmannite based on the ideal formula of Walenta (1976).

\* The content of carbon dioxide was calculated from the ideal formula and CO<sub>2</sub> made equal to the ratio of 1:3 U/C in the uranyl tricarbonate ion.

TABLE 4. Chemical composition of widenmannite II.

	1	2	3	4	5	Mean	Ideal
PbO	51.81	47.08	48.16	46.23	51.81	48.78	51.64
ZnO	0.07	0.61	0.31	0.04	0.07	0.26	0.00
UO <sub>3</sub>	34.66	34.22	34.24	34.70	34.66	34.62	33.09
CO <sub>2</sub> *	16.00	15.78	15.80	16.00	16.80	15.98	15.27
Total	102.54	97.69	98.51	96.97	103.34	99.63	100.00
Formula based on $\Sigma(\text{Pb}+\text{Fe}+\text{Zn}+\text{U}) = 3$							
Pb	1.966	1.872	1.908	1.889	1.952	1.913	2.000
Zn	0.007	0.067	0.034	0.004	0.032	0.028	0.000
$\Sigma A$ site	1.973	1.939	1.942	1.893	1.984	1.941	2.000
U	1.026	1.061	1.058	1.107	1.016	1.059	1.000
C*	3.080	3.181	3.174	3.316	3.053	3.178	3.000
$\Sigma(\text{U}+\text{C})$	4.106	4.243	4.232	4.422	4.069	4.237	4.000
Pb/U	1.92	1.76	1.80	1.71	1.92	1.81	2.00

Mean: based on 35 point analyses.

Ideal: theoretical composition of widenmannite based on ideal formula of Walenta (1976).

\* The content of carbon dioxide was calculated from the ideal formula and CO<sub>2</sub> made equal to the ratio of 1:3 U/C in the uranyl tricarbonate ion

1–5 representative analyses

average results of 35 spot analyses based on the same basis as above is  $(\text{Pb}_{1.91}\text{Zn}_{0.03})_{\Sigma 1.94}(\text{UO}_2)_{1.06}(\text{CO}_3)_{3.18}$  (Table 4). Apart from the dominant Pb in the cationic site, small quantities of Zn were also observed. The contents of Zn and Pb correlate very well (Fig. 2) and are independent of the U content.

According to the thermal study, widenmannite II decomposes in several partly-overlapping steps (Fig. 3; Table 5):  $\sim 0.5 \text{ CO}_2$  ( $\rightarrow 320^\circ\text{C}$ ),  $\sim 0.5 \text{ CO}_2$  ( $\rightarrow 420^\circ\text{C}$ ),  $\sim 2 \text{ CO}_2$  ( $\rightarrow 460^\circ\text{C}$ ). The release of the remaining CO<sub>2</sub> and O<sub>2</sub> takes place up to 880°C. The total weight loss ( $\sim 15 \text{ wt.}\%$ ) corresponds to the total content of  $(\text{CO}_3)^{2-}$  anions which could

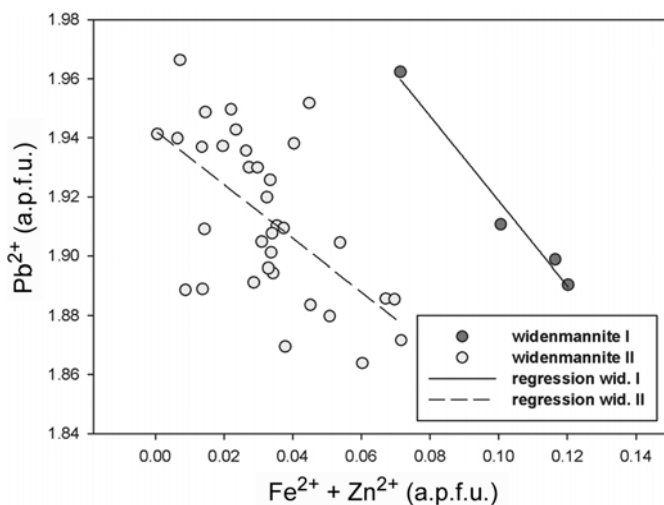


FIG. 2. An a.p.f.u. binary plot of Fe+Zn vs Pb in the A-site of widenmannite I and II.

WIDENMANNITE FROM PŘÍBRAM, CZECH REPUBLIC

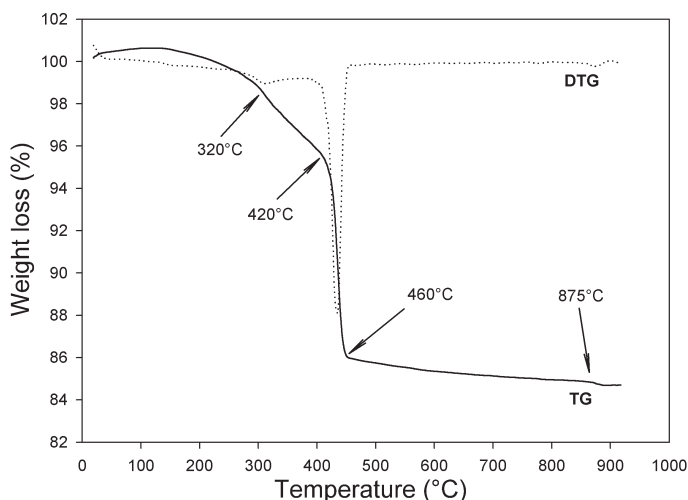


FIG. 3. TG and DTG curves of widenmannite.

not be measured directly by EPMA. Adsorbed water and hydroxyls (their presence is concluded from the vibration spectra) are released at the beginning of the first decomposition step. Widenmannite decomposition can be described simply as:  $\text{Pb}_2\text{UO}_2(\text{CO}_3)_3 \rightarrow [\text{Pb}_2\text{UO}_2(\text{CO}_3)_{2.5}] \rightarrow [\text{Pb}_2\text{UO}_2(\text{CO}_3)_2] \rightarrow [2\text{PbO} \cdot \text{UO}_3] \rightarrow [\text{Pb}_2\text{UO}_x]$  ( $x < 5$ ).

*Vibrational spectra*

Widenmannite contains  $\text{Pb}^{2+}$ ,  $(\text{UO}_2)^{2+}$  and  $(\text{CO}_3)^{2-}$  ions in its crystal structure. A free uranyl ion,  $(\text{UO}_2)^{2+}$ ,  $D_{\infty h}$  point-group symmetry, exhibits four normal vibrations:  $\nu_1$  symmetric stretching vibration (Raman active,

$900\text{--}750\text{ cm}^{-1}$ );  $\nu_2(\delta)$  doubly degenerate bending vibration (IR active,  $300\text{--}200\text{ cm}^{-1}$ );  $\nu_3$  antisymmetric stretching vibration (IR active,  $1000\text{--}850\text{ cm}^{-1}$ ). The lowering of symmetry ( $D_{\infty h} \rightarrow C_{\infty v}$ ,  $C_{2v}$  or  $C_s$ ) causes activation of all three modes both in the IR and Raman spectra. In such cases the  $\nu_2$  vibration usually splits into two IR- and Raman-active components (Čejka, 1999). The free planar  $(\text{CO}_3)^{2-}$  group of point-group symmetry  $D_{3h}$  exhibits six normal vibrations:  $\nu_1$  symmetric stretching vibration, (Raman active,  $1115\text{--}1050\text{ cm}^{-1}$ );  $\nu_2$  out-of-plane bending vibration, (IR active,  $880\text{--}835\text{ cm}^{-1}$ );  $\nu_3$  doubly degenerate antisymmetric stretching vibration (both IR and Raman active,  $1610\text{--}1250\text{ cm}^{-1}$ );  $\nu_4$  doubly degenerate in-plane bending vibration,

TABLE 5. Results of thermal analysis of widenmannite II from Příbram.

Step	Temperature (°C)	Weight loss (mg)	Weight (%)	Mass units	Interpretation
1	320	0.021	2.534	21.972	0.499 CO <sub>2</sub> ~0.5 CO <sub>2</sub>
2	420	0.019	2.353	20.167	0.458 CO <sub>2</sub> ~0.5 CO <sub>2</sub>
3	460	0.078	9.470	82.112	1.866 CO <sub>2</sub>
4*	875	0.008	0.995	8.627	0.196 CO <sub>2</sub> 2.062 CO <sub>2</sub> ~2 CO <sub>2</sub> Σ3.019 CO <sub>2</sub> ~3 CO <sub>2</sub>
5*	880	0.001	0.180	1.561	~0.1 O <sub>2</sub>
Total		0.127	15.532	134.439	

\* Steps 4 and 5 may overlap as a result of release of the rest of CO<sub>2</sub> and oxygen.

(both IR and Raman active, 770–670  $\text{cm}^{-1}$ ). In the case of lowering the symmetry ( $D_{3h} \rightarrow C_{3v}$ ,  $C_s$  or  $C_1$ ), all vibrations become IR- and Raman-active and  $\nu_3$  and  $\nu_4$  vibrations are split. The  $(\text{CO}_3)^{2-}$  anion behaves as a monodentate or bidentate ligand and tends, therefore, to be coordinated to  $\text{U}^{6+}$  mono- or bidentately in its equatorial plane. This ligancy can be inferred from the difference between the wavenumbers of the split  $\nu_3(\text{CO}_3)^{2-}$  vibrations: splitting is larger for the bidentate than in the monodentate state (Čejka, 1999). For the large  $f$  transition metals,  $\nu_3$  splitting can be calculated to be 50–60  $\text{cm}^{-1}$  in

monodentate- and 160–190  $\text{cm}^{-1}$  in bidentate structures (Jolivet *et al.*, 1980).

Tentative interpretation of the IR and Raman spectra of widenmannite (Table 6) was based on the Anderson study of  $\text{K}_4[\text{UO}_2(\text{CO}_3)_3]$  (Anderson *et al.*, 1980) and Koglin's paper on  $\text{Na}_4[\text{UO}_2(\text{CO}_3)_3]$  (Koglin *et al.*, 1979). An infrared spectrum of widenmannite was published for the first time by Elton and Hooper (1995) without any detailed interpretation. Even if Walenta (1976) described widenmannite as anhydrous lead uranyl tricarbonate,  $\text{Pb}_2\text{UO}_2(\text{CO}_3)_3$ , the IR spectrum of Elton and

TABLE 6. Infrared absorption and Raman data for widenmannite II from Příbram with tentative assignment.

Infrared spectrum ( $\text{cm}^{-1}$ )	Raman spectrum ( $\text{cm}^{-1}$ )	Assignment
	3592 w sh 3568 m 3078 m	$\nu\text{OH}$ stretch
3559 w-m		
1517 vs	1509 w 1470 w	$\nu_3(\text{CO}_3)^{2-}$ antisymmetric stretch
1394 s	1381 m	
1351 m-s	1348 w	
	1122 m	$\nu_1(\text{CO}_3)^{2-}$ symmetric stretch and/or $\delta\text{U}-\text{OH}$ ( $\delta\text{Pb}-\text{OH}?$ ) bend
	1068 m 1058 w	
1058 w		
926 s		$\nu_3(\text{UO}_2)^{2+}$ antisymmetric stretch
856 w-m	849 s	$\nu_1(\text{UO}_2)^{2+}$ symmetric stretch and/or $\nu_2(\delta_2)(\text{CO}_3)^{2-}$ out-of-plane bend
828 w-m		
	736 vw	$\nu_4(\delta_4)(\text{CO}_3)^{2+}$ in-plane bend
728 m		
653 w-m	725 m	
	355 m	$\nu(\text{U}-\text{O}_{\text{ligand}})$
	268 m	$\nu_2(\delta)(\text{UO}_2)^{2+}$ bend
	246 m	
	225 m 211 w 191 m	$(\text{CO}_3)^{2-}$ librations
	128 vvw 115 vw	$(\text{UO}_2)^{2+}$ librations

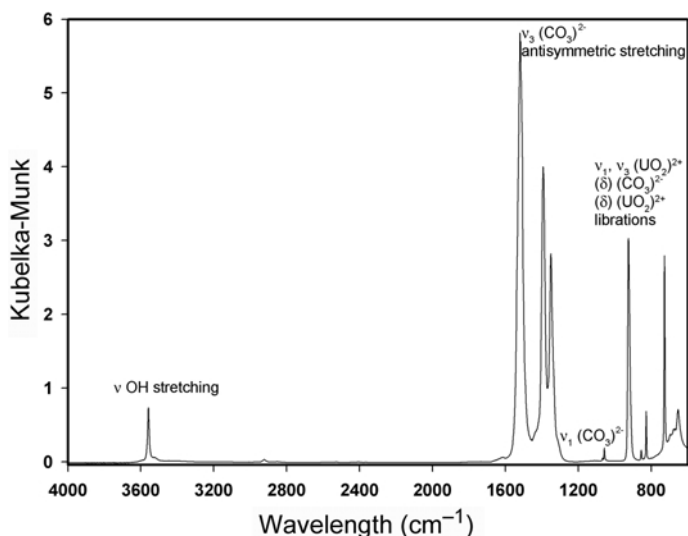


FIG. 4. Infrared (DRIFT) spectrum of widemannite with assigned vibration regions.

Hooper's widemannite suggests the presence of molecular water ( $\nu$ OH stretching vibrations at 3561 and 3457  $\text{cm}^{-1}$  and  $\delta\text{H}_2\text{O}$  bending vibration at 1620  $\text{cm}^{-1}$ ). However, this water likely comes from wet-KBr used in the preparation of the pellets. The infrared spectrum of widemannite II presented in the current study is similar to that published by Elton and Hooper (1995). However, we find no evidence of the bands attributable to vibrations of water molecules in our sample.

In the IR and Raman spectra of the widemannite sample, a sharp band can be observed at 3559  $\text{cm}^{-1}$  with a shoulder at 3592  $\text{cm}^{-1}$  (IR) (Fig. 4) and at 3568  $\text{cm}^{-1}$  and 3078  $\text{cm}^{-1}$  (Raman) (Fig. 5d). These bands may be related to the OH-stretching vibrations. However, no bands were observed close to 1630  $\text{cm}^{-1}$ , which is characteristic for  $\delta\text{H}_2\text{O}$  bending modes. Based on this fact, the bands adhere to  $\nu$ OH stretching vibrations of weakly bonded hydroxyls (Libowitzky, 1999).

An infrared band at 926  $\text{cm}^{-1}$  (Fig. 4) is assigned to the  $\nu_3(\text{UO}_2)^{2+}$  antisymmetric stretching vibration. This frequency corresponds to the U–O bond length in uranyl of 1.77 Å (calculated with the empirical relation  $R_{\text{U-O}} = 91.41\nu_3^{-2/3} + 0.804$  Å by Bartlett and Cooney, 1989) or 1.78 Å (empirical relation  $R_{\text{U-O}} = 65.356\nu_3^{-2/3} + 1.088$  Å by Čejka, 2005). This band is not present in the Raman spectrum of widemannite. Bands at 856 and 828  $\text{cm}^{-1}$  (IR)

(Fig. 4), and at 849  $\text{cm}^{-1}$  (Raman) (Fig. 5a) are attributed to the  $\nu_1(\text{UO}_2)^{2+}$  symmetric stretching vibrations. However, the  $\nu_1(\text{UO}_2)^{2+}$  is probably overlapped by the  $\nu_2(\delta_2)(\text{CO}_3)^{2-}$  out-of-plane bending vibration and/or a  $\delta\text{U-OH}$  (or  $\delta\text{Pb-OH}$ ?) bending vibration. Inferred U–O bond lengths in uranyl (empirical relation  $R_{\text{U-O}} = 106.5\nu_1^{-2/3} + 0.575$  Å by Bartlett and Cooney, 1989) are 1.76 Å (856  $\text{cm}^{-1}$ /IR), 1.78 Å (828  $\text{cm}^{-1}$ /IR) and 1.76 Å (849  $\text{cm}^{-1}$ /Raman). All inferred bond-lengths are consistent with the values reported for the natural and synthetic uranyl compounds, including uranyl carbonates that contain hexagonal dipyramidal uranyl coordination polyhedra (Burns, 1999, 2005; Burns *et al.*, 1996, 1997).

Bands at 1351, 1394 and 1517  $\text{cm}^{-1}$  (IR) (Fig. 4) and 1348, 1381, 1470, 1509  $\text{cm}^{-1}$  (Raman) (Fig. 5a,c) are attributable to the split  $\nu_3(\text{CO}_3)^{2-}$  antisymmetric stretching vibration. The value of this splitting ( $\Delta\nu = 166$   $\text{cm}^{-1}$ ) supports the conclusion that carbonate ions are bidentately bonded to the equatorial plane of the  $(\text{UO}_2)^{2+}$ , thus forming the well known uranyl tricarboxylate complex anion  $[\text{UO}_2(\text{CO}_3)_3]^{4-}$  (Jolivet *et al.*, 1980; Dik *et al.*, 1989) in which the uranyl hexagonal dipyramidal coordination polyhedron occurs. Bands at 1058  $\text{cm}^{-1}$  (IR) and 1058  $\text{cm}^{-1}$  (Raman) are attributed to the  $\nu_1(\text{CO}_3)^{2-}$  symmetric stretching vibration. Bands at 1122 and 1068  $\text{cm}^{-1}$  (Raman) may be connected with

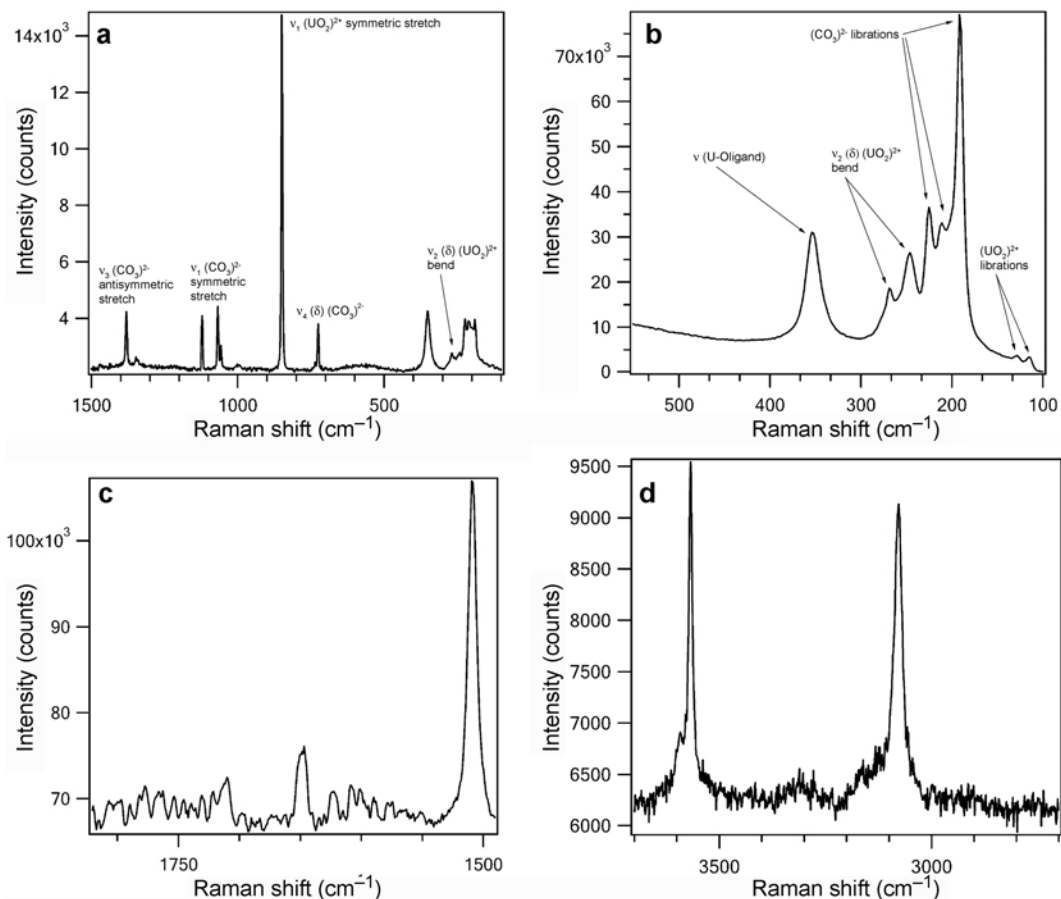


FIG. 5. Raman spectra of widemannite: (a) 100–1500  $\text{cm}^{-1}$ . (b) 100–500  $\text{cm}^{-1}$ . (c) 1500–1800  $\text{cm}^{-1}$  (double degenerate  $\nu_3(\text{CO}_3)^{2-}$  antisymmetric stretching vibration). (d) 3000–3500  $\text{cm}^{-1}$  ( $\nu\text{OH}$  stretching region).

the  $\delta\text{U}-\text{OH}$  or  $\delta\text{Pb}-\text{OH}$  bending vibrations. As mentioned above, bands at 856 (IR) and 849 (Raman)  $\text{cm}^{-1}$  were assigned to the  $\nu_1(\text{UO}_2)^{2+}$  symmetric stretching vibrations. However, an overlap of the  $\nu_1(\text{UO}_2)^{2+}$  symmetric stretching vibration with the  $\nu_2(\delta_2)(\text{CO}_3)^{2-}$  out-of-plane bending vibration or  $\delta\text{U}-\text{OH}$  bending vibration is highly probable in the infrared spectrum. The split  $\nu_4(\delta_4)(\text{CO}_3)^{2-}$  in-plane bending vibration was observed as bands at 728 and 653  $\text{cm}^{-1}$  (IR) (Fig. 4) and 736 and 725  $\text{cm}^{-1}$  (Raman) (Fig. 5a). A band at 353  $\text{cm}^{-1}$  (Raman) may probably be assigned to the  $\nu(\text{U}-\text{O}_{\text{ligand}})$  vibration, and those at 268 and 246  $\text{cm}^{-1}$  (Raman) to the split  $\nu_2(\delta)(\text{UO}_2)^{2+}$  bending vibration (Fig. 5b). According to Anderson *et al.* (1980), Raman bands at 225, 211 and 191  $\text{cm}^{-1}$  and 128 and 115

$\text{cm}^{-1}$  may be assigned to the  $(\text{CO}_3)^{2-}$  and  $(\text{UO}_2)^{2+}$  librations respectively (Fig. 5b).

#### Lead isotopes

There are two possible sources of Pb in widemannite: uraninite, which contains two radiogenic isotopes,  $^{207}\text{Pb}$  and  $^{206}\text{Pb}$ ; and galena, containing the non-radiogenic (thoro-genic) isotope  $^{208}\text{Pb}$ . The following two Pb isotope ratios,  $^{207}\text{Pb}/^{206}\text{Pb}$  and  $^{208}\text{Pb}/^{206}\text{Pb}$ , were used for the determination of the Pb source in the studied widemannite. Analytical results are presented in Table 7. The estimation of the primary U mineralization age, the isotopic composition of average galena from the Březové Hory deposit and uraninite from the Jánská vein were reported recently by Škácha *et al.*

## WIDENMANNITE FROM PŘÍBRAM, CZECH REPUBLIC

 TABLE 7. Results of the mass spectrometry of Pb isotopes and  $\alpha$  spectrometry of radionuclides in the widenmannite samples.

	Widenmannite I	Widenmannite II
$^{207}\text{Pb}/^{206}\text{Pb}$	0.8490±0.0118	0.8470±0.0060
$^{208}\text{Pb}/^{206}\text{Pb}$	2.0807±0.0276	2.0633±0.0214
calc. radiogenic lead (%) $^{207}\text{Pb}/^{206}\text{Pb}$	1.655±0.024	1.902±0.014
calc. radiogenic lead (%) $^{208}\text{Pb}/^{206}\text{Pb}$	1.154±0.016	1.980±0.020
U ( $^{238}\text{U}$ ) (Bq g <sup>-1</sup> )	4009±434	2690±352
$^{226}\text{Ra}$ ( $^{214}\text{Po}$ ) (Bq g <sup>-1</sup> )	1278±147	8.9±4.2
$^{210}\text{Pb}$ ( $^{210}\text{Po}$ ) (Bq g <sup>-1</sup> )	1425±172	67.1±16.4
$^{230}\text{Th}/^{234}\text{U}$	0.933±0.074	n.a.
$^{234}\text{U}/^{238}\text{U}$	0.960±0.025	n.a.
Age (±2 $\sigma$ )	>222,000 y	118.1±11.9

Activities of  $^{238}\text{U}$ ,  $^{226}\text{Ra}$  and  $^{210}\text{Po}$  (measured on the  $\alpha$  spectrum) were estimated by the method of non-destructive spectrometry (powder sample). The values of the isotope ratios were measured after chemical separation of isotopes. All errors are expressed as 2 $\sigma$ ; the substantial contribution to the error of non-destructive spectroscopy is due to weighing inaccuracies.

*al.* (2009). The concentration of radiogenic Pb incorporated in the particular secondary phase can be determined based on the model of binary mixing between outer members (radiogenic and non-radiogenic) and experimental observed values. In both types of widenmannite, the portion of radiogenic Pb is negligible at ~1–2% (Table 7).

#### Alpha spectrometry

To evaluate the possible radionuclide equilibrium and to check the possibility of dating using

radiogenic isotopes, both types of widenmannite were analysed by alpha spectrometry. The analytical methods are described in the Experimental Methods section and the analytical results are presented in Table 7 and Fig. 6.

The experimental spectrum (Fig. 6a) of widenmannite I exhibits long-lived  $^{238}\text{U}$ ,  $^{234}\text{U}$ ,  $^{230}\text{Th}$  and  $^{226}\text{Ra}$  radionuclides. Together, weak activities of  $^{222}\text{Rn}$  and its short-lived daughters ( $^{218}\text{Po}$  and  $^{214}\text{Po}$ ) and  $^{210}\text{Pb}$  relatively long-lived, are also clearly visible. It suggests a long-term escape of  $^{222}\text{Rn}$  ( $^{222}\text{Rn}$  and  $^{210}\text{Pb}$  equilibrium) due to

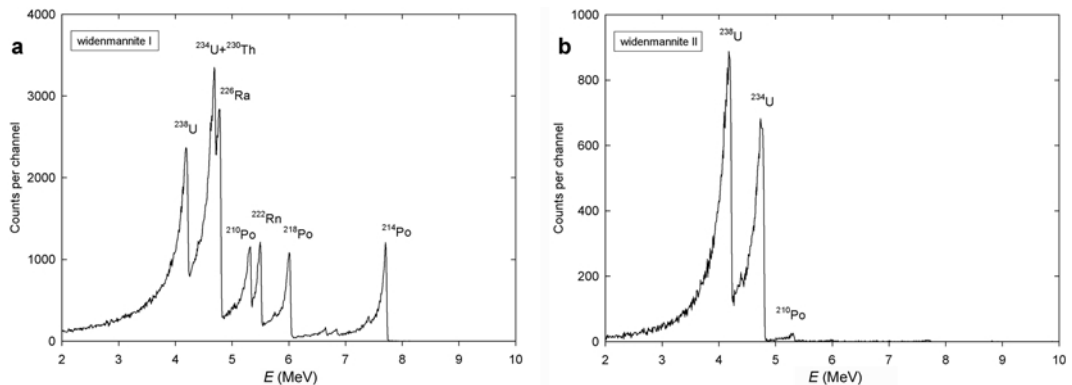


FIG. 6. Alpha spectrum of the widenmannite powdered samples: (a) widenmannite I, mass 200±10  $\mu\text{g}$ , counting time 70.9 h, suggests close  $^{226}\text{Ra}/^{238}\text{U}$  radioactive equilibrium, partial radon loss is evident; (b) widenmannite II, mass 194±11  $\mu\text{g}$ , counting time 38.6 h, recently formed, both U isotopes and small amount of  $^{210}\text{Po}$  ( $^{210}\text{Pb}$  daughter) are present.

sample porosity. It enables us to calculate the percentage of the Rn remaining in the mineral ( $A_{222\text{Rn}}$  (measured as  $^{214}\text{Po}$ )/ $A_{238\text{U}} * 100$ ) = 31.9%, or it can be calculated from the  $^{210}\text{Pb}$  daughter ( $A_{210\text{Pb}}$  (measured as  $^{210}\text{Po}$ )/ $A_{238\text{U}} * 100$ ) = 35.5% in the same manner. The input values are presented in Table 7.

The continual Rn loss or long-term Rn influx into non-U porous secondary minerals (such as opal or recently-formed carbonates) can disturb their U/Pb or stable Pb/Pb isotopic systems and can influence strongly their isotopic ages (Neymark and Amelin, 2008).

For dating of the unsaturated zone (the open systems), the  $^{230}\text{Th}/^{234}\text{U}$  (Th-U) method is widely employed. The Rn loss in this case is unimportant for further calculation because both  $^{230}\text{Th}$  and  $^{234}\text{U}$  are precursors in the U decay chain. This method was applied successfully to the dating of secondary U minerals (Löfvendahl and Holm, 1981), speleothems (Richards and Dorale, 2003) and surface hot-spring carbonate sediments (Vylita *et al.*, 2007).

The sample of widenmannite I was dated by  $^{230}\text{Th}/^{234}\text{U}$ . The age and initial  $^{234}\text{U}/^{238}\text{U}$  ratio of widenmannite I were calculated using the equation of Richards and Dorale (2003). It lies within an equilibrium (Table 7), therefore the minimal age was calculated based on  $^{230}\text{Th}/^{234}\text{U}$  ratio minus  $2\sigma$ . The sample indicates an age >222,000 y.

The alpha spectrum of widenmannite II is completely different from that of widenmannite I (Fig. 6b). It suggests the presence of predominantly  $^{234}\text{U}$  and  $^{238}\text{U}$  isotopes. Additionally,  $^{210}\text{Po}$  occurs as a minor radionuclide. The isotopes  $^{226}\text{Ra}$ ,  $^{222}\text{Rn}$  and their short-lived daughters are present only in traces in this case.

From the equilibrium observed, it can be inferred that widenmannite II is very young. The half-life of  $^{210}\text{Pb}$  is only 22.3 y and it is unsupported by the  $^{226}\text{Ra}$  parent activity. To calculate the  $^{210}\text{Pb}$  model-age, the following data have to be available: (1) the  $^{210}\text{Pb}$  activity of the fresh radiogenic Pb and (2) the initial  $^{210}\text{Pb}$  activity of a particular phase – in our case widenmannite II. Both values can be deduced easily from the alpha- and mass spectrometry of Pb isotopes (Table 7):

(1) The primary uraninite from the Jánská vein contains 3.32 wt.% of radiogenic Pb (mean of three F-AAS results), and 74.89 wt.% of U (mean of three ICP-MS results). In the equilibrium state, the activity of  $^{210}\text{Pb}$  in uraninite will be equal to the  $^{238}\text{U}$  parent, e.g. 9250 Bq  $\text{g}^{-1}$  (1 mg U  $\equiv$

12.35 Bq). The activity of pure radiogenic Pb will therefore be 278,279 Bq  $\text{g}^{-1}$  of  $^{210}\text{Pb}$ .

(2) Initial  $^{210}\text{Po}$  activity of widenmannite II can be calculated based on the idea of the mixing of radiogenic and common Pb isotopes. The measured portion of pure radiogenic Pb in widenmannite II is 1.94% (average of both Pb isotope ratios, Table 7); the total Pb content is 39.64 wt.% (F-AAS results). The widenmannite II calculated initial activity  $A_0$  is 2140 Bq  $\text{g}^{-1}$ .

The unsupported activity of  $^{210}\text{Po}$  (calculated as  $A_{210\text{Po}} - A_{226\text{Ra}}$ ) is  $58.3 \pm 20.5$  Bq  $\text{g}^{-1}$ . The resulting  $^{210}\text{Pb}$  model-age of widenmannite II sample is  $118.1 \pm 11.9$  y (Table 7). Assuming recycled radiogenic Pb present in the minerals studied, the widenmannite sample may be younger than the measured data indicate.

## Discussion and conclusions

An ideal formula of widenmannite reported by Walenta (1976),  $\text{Pb}_2(\text{UO}_2)(\text{CO}_3)_3$ , was confirmed by the electron microprobe (Tables 3, 4). Even if the composition obtained differs in the empirical Pb/U ratio and in presence of minor isomorphous portions of Fe and Zn, the IR and Raman spectra prove that widenmannite contains no molecular water bonded in the crystal structure: no bands related to the  $\nu_2(\delta)\text{H}_2\text{O}$  bending vibration were observed. However, the presence of some bands in the region of the OH-stretching vibration and  $\delta\text{U}-\text{OH}$  (or  $\delta\text{Pb}-\text{OH}$ ) in the region of the  $\nu_1$  and  $\nu_2(\delta_2)(\text{CO}_3)^{2-}$  vibrations indicate that hydroxyls may substitute carbonate ions in the crystal structure of widenmannite.

Alpha- and mass spectrometry of U and Pb isotopes enable us to distinguish two different generations of widenmannite. These two generations were formed under different conditions. The older widenmannite I was probably formed as a long-term *in situ* alteration product of the weathering of primary mineralization (galena and uraninite) by meteoric descending water. The low  $^{234}\text{U}/^{238}\text{U}$  isotopic ratio implies strong leaching of the primary association (Chabaux *et al.*, 2003). In contrast, the younger widenmannite II was formed by dissolution of the primary U and Pb minerals in the environment of the open adit. It occurs in the open cracks of galena, sphalerite, quartz and rare uraninite at the top of the adit walls. The association of U and base-metal mineralization (primarily galena) is a characteristic feature of the Jánská vein. The major portion of Pb incorporated in widenmannite originates

from galena as indicated by the small contents of radiogenic Pb in the widenmannite from the Jánská vein.

### Acknowledgements

The authors thank M. Mazuch (Faculty of Science, Charles University in Prague) for his help with obtaining SE images on the scanning electron microscope, M. Fayadová and O. Šebek (Faculty of Science, Charles University in Prague) for their help in the laboratory. Our special thanks are due to J. Ederová (Institute of Chemical Technology, Praha) for performing thermal analyses. This study was supported financially by the Grant Agency of the Academy of Sciences of the Czech Republic (project KJB 301110602), Ministry of Culture of the Czech Republic (project MK00002327201) and Ministry of Education (MSM 0021620855) and by an internal project of the Czech Geological Survey (project no. 323000).

### References

- Anderson, A., Chieh, C., Irish, D.E. and Tong, J.P.K. (1980) An X-ray crystallographic, Raman, and infrared spectral study of crystalline potassium uranyl carbonate,  $K_4UO_2(CO_3)_3$ . *Canadian Journal of Chemistry*, **58**, 1651–1658.
- Babánek, F. (1872) Zur Paragenese der Příbramer Mineralien. *Jahrbuch der kaiser-königliche geologische Reichsanstalt* (Wien), **22**, 27–39. (in German).
- Bartlett, J.R. and Cooney, R.P. (1989) On the determination of uranium-oxygen bond lengths in dioxouranium(VI) compounds by Raman spectroscopy. *Journal of Molecular Structure*, **193**, 295–300.
- Burnham, Ch.W. (1962) Lattice constant refinement. *Carnegie Institute of Washington Year Book*, **61**, 132–135.
- Burns, P.C. (1999) The crystal chemistry of uranium. Pp. 23–90 in: *Uranium: Mineralogy, Geochemistry and the Environment* (P.C. Burns and R. Finch, editors). Reviews in Mineralogy, **38**, Mineralogical Society of America, Chantilly, Virginia, USA.
- Burns, P.C. (2005)  $U^{6+}$  minerals and inorganic compounds: insights into an expanded structural hierarchy of crystal structures. *The Canadian Mineralogist*, **43**, 1839–1984.
- Burns, P.C., Miller, M.L. and Ewing, R.C. (1996)  $U^{6+}$  minerals and inorganic phases: A comparison and hierarchy of crystal structures. *The Canadian Mineralogist*, **34**, 845–880.
- Burns, P.C., Ewing, R.C. and Hawthorne, F.C. (1997) The crystal chemistry of hexavalent uranium: Polyhedron geometries, bond-valence parameters, and polymerization of polyhedra. *The Canadian Mineralogist*, **35**, 1551–1570.
- Carlson, M.S., Robinson, W.G., Elder, J.M., Jaszczak, A.J. and Bornhorst, J.T. (2007) Greenockite and associated uranium – vanadium minerals from the Huron River uranium prospect, Baraga County, Michigan. *Rocks & Minerals*, **82**, 298–308.
- Čejka, J. (1999) Infrared spectroscopy and thermal analysis of the uranyl minerals. Pp. 521–622 in: *Uranium: Mineralogy, Geochemistry and the Environment* (P.C. Burns and R. Finch, editors). Reviews in Mineralogy, **38**, Mineralogical Society of America, Chantilly, Virginia, USA.
- Čejka, J. (2005) Vibrational spectroscopy of the uranyl minerals – infrared and Raman spectra of the uranyl minerals II. Uranyl carbonates. *Bulletin mineralogicko-petrologického oddělení Národního Muzea* (Praha), **13**, 62–72. (in Czech).
- Chabaux, F., Riotte J. and Dequincey, O. (2003) U-Th-Ra fractionation during weathering and river transport. Pp. 533–576 in: *Uranium-series Geochemistry*. (B. Bourdon, G.M. Henderson, C.C. Lundstrom and S.P. Turner, editors). Reviews in Mineralogy, **52**, Mineralogical Society of America, Chantilly, Virginia, USA.
- Cheary, R.W. and Coelho, A.A. (1996) *Programs XFIT and FOURYA*, Deposited in CCP14 Powder Diffraction Library, Engineering and Physical Sciences Research Council, Daresbury Laboratory, Warrington, UK.
- Dik, T.A., Umreyko, D.S., Nikanovich, M.V. and Klavstut', G.N. (1989) Coordination influence on spectral characteristics of  $CO_3^{2-}$  anion in uranyl carbonate complexes. *Koordinatsionnaya Khimiya*, **15**, 225–231. (in Russian).
- Elton, N.J. and Hooper, J.J. (1995) Widenmannite from Cornwall, England: the second world occurrence. *Mineralogical Magazine*, **59**, 745–749.
- Elton, N.J. and Hooper, J.J. (1996) A further occurrence of widenmannite in Cornwall, England (North Zawn, St Just.). *Journal of the Russell Society*, **6**, 98.
- Halls, Ch. (2005) *Report on the mineralogy of a sample from the Agricola Resources Energy Ridge Prospect, Hautuajaervi, Lapin Laani, Finland*. Final Report, Department of Mineralogy, NHM, London, pp. 1–24.
- Jarka, P. (2007) *Uran-polymetallic mineralization of the Jánská vein, Příbram-Březové Hory, ČR: Alpha spectrometric determination of radionuclides*. MSc thesis (MS), Charles University in Prague, 45 pp. (in Czech).
- Jolivet, J.P., Thomas, Y. and Taravel, B. (1980) Vibrational study of coordinated  $CO_3^{2-}$  ions. *Journal of Molecular Structure*, **60**, 93–98.

- Killeen, P.G. and Carmichael, C.M. (1976) Determination of radioactive disequilibrium in uranium ores by alpha-spectrometry. *Papers of Geological Survey of Canada*, **75** (38), 1–17.
- Koglin, E., Schenk, H.J. and Schwochau, K. (1979) Vibration and low temperature spectra of the uranyl tricarbonate complex  $[\text{UO}_2(\text{CO}_3)_3]^{4-}$ . *Spectrochimica Acta*, **35A**, 641–647.
- Le Bail, A. (1998) *HKLGEn: A program for generating hkl, multiplicity, d(hkl), 2-theta from a wavelength, a space group, cell parameters*. Deposited in CCP14 Powder Diffraction Library, Engineering and Physical Sciences Research Council, Daresbury Laboratory, Warrington, UK (<http://www.ccp14.ac.uk/ccp/web-mirrors/armel/www.cristal.org/>).
- Libowitzky, E. (1999) Correlation of O–H stretching frequencies and O–H··O hydrogen bond lengths in minerals. *Monatshefte für Chemie*, **130**, 1047–1059.
- Löfvendahl, R. and Holm, E. (1981) Radioactive disequilibria and apparent ages of secondary uranium minerals in Sweden. *Lithos*, **14**, 189–201.
- Maxwell, S.L. (1998) Rapid actinide-separation methods. *Radioactivity and Radiochemistry*, **8**, 36–44.
- Mihaljevič, M., Zuna, M., Ettlér, V., Šebek, O., Strnad, L. and Goliáš, V. (2006) Lead fluxes, isotopic and concentration profiles in a peat deposit near a lead smelter (Příbram, Czech Republic). *Science of the Total Environment*, **372**, 334–344.
- Neymark, L.A. and Amelin, Y.V. (2008) Natural radionuclide mobility and its influence on U-Th-Pb dating of secondary minerals from the unsaturated zone at Yucca Mountain, Nevada. *Geochimica et Cosmochimica Acta*, **72**, 2067–2089.
- Ondruš, P. and Hyršl, J. (1989) New finds and revision of the secondary minerals from Příbram district. *Acta Universitatis Carolinae* (Prague), Geologica, Čech Vol., 521–533.
- Plášil, J., Škácha, P. and Sejkora, J. (2003) Neufunde auf dem Johannes-Gang, Revier Birkenberg, Příbram (CZ). *Lapis*, **28**, 71–72. (in German).
- Plášil, J., Sejkora, J., Škácha, P., Goliáš, V. and Hušák, M. (2005) Compreignacite, uranophane and uranopillite from the Jánská vein, Březové Hory, Příbram. *Bulletin mineralogicko-petrologického Oddělení Národního Muzea* (Praha), **13**, 192–195. (in Czech).
- Plášil, J., Sejkora, J., Čejka, J., Škácha, P., Goliáš, V. and Ederová, J. (2010) Characterization of phosphate rich metaloděvite from Příbram, Czech Republic. *The Canadian Mineralogist*, **48**, 113–122.
- Pouchou, J.L. and Pichoir, F. (1985) ‘PAP’  $\phi(\rho Z)$  procedure for improved quantitative microanalysis. Pp. 104–106 in: *Microbeam Analysis* (J.T. Armstrong, editor). San Francisco Press, San Francisco, California, USA.
- Reuss, E.A. (1859) Mineralogische Notizen aus Böhmen. *Lotos* (Wien) **9**, 51–56. (in German).
- Reuss, E.A. (1863) Über die Paragenese der auf den Erzgangen von Příbram einbrechenden Mineralien. *Sitzungsberichte der Kaiserlichen Akademie der Wissenschaften*, (Wien), **47**, 13–76. (in German).
- Richards, D.A. and Dorale, J.A. (2003) Uranium-series chronology and environmental applications of speleothems. Pp. 407–460 in: *Uranium-series Geochemistry*. (B. Bourdon, G.M. Henderson, C.C. Lundstrom and S.P. Turner, editors). Reviews in Mineralogy and Geochemistry, **52**, Mineralogical Society of America, Chantilly, Virginia, USA.
- Sejkora, J. and Gabašová, A. (1995) Nesquehonite and widenmannite from Jáchymov. *Bulletin mineralogicko-petrologického Oddělení Národního Muzea* (Praha), **3**, 241. (in Czech).
- Sejkora, J., Čejka, J., Škácha, P., Gabašová, A. and Novotná, M. (2003) Minerals of the zippeite group from the Jánská vein, Březové Hory, Příbram. *Bulletin mineralogicko-petrologického Oddělení Národního Muzea* (Praha), **11**, 183–189. (in Czech).
- Škácha, P. and Plášil, J. (2002) Minerals of the Březové Hory ore district. *Bulletin mineralogicko-petrologického Oddělení Národního Muzea* (Praha), **10**, 43–77. (in Czech).
- Škácha, P. and Sejkora, J. (2001) Kasolite from the Jánská vein, Březové Hory, Příbram. *Bulletin mineralogicko-petrologického Oddělení Národního Muzea* (Praha), **9**, 272–273. (in Czech).
- Škácha, P., Goliáš, V., Sejkora, J., Plášil, J., Strnad, L., Škoda, R. and Ježek, J. (2009) Hydrothermal uranium-base metal mineralization of the Jánská vein, Březové Hory, Příbram, Czech Republic: Lead isotopes and chemical dating of uraninite. *Journal of Geosciences*, **54**, 1–13.
- Strnad, L., Mihaljevič, M. and Šebek, O. (2005) Laser ablation and solution ICP-MS determination of REE in USGS BIR-1G, BHVO-2G and BCR-2G glass reference materials. *Geostandards Newsletter - the Journal of Geostandards and Geoanalysis*, **29**, 303–314.
- Vylita, T., Žák, K., Cílek, V., Hercman, H. and Mikšíková, L. (2007) Evolution of hot-spring travertine accumulation in Karlovy Vary/Carlsbad (Czech Republic) and its significance for the evolution of Teplá valley and Ohře/Eger rift. *Zeitschrift für Geomorphologie*, **51**, 427–442.
- Walenta, K. (1976) Widenmannit und Joliotit, zwei neue Uranylkarbonatminerale aus dem Schwarzwald. *Schweizerische Mineralogische und Petrographische Mitteilungen*, **56**, 167–185. (in German).